PAPER

The isotropic emission of tribo-generated x-rays from peeling adhesive tape

View the article online for updates and enhancements.
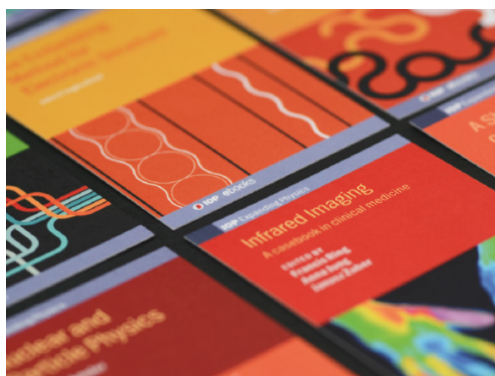
The isotropic emission of tribo-generated x-rays from peeling adhesive tape

M C Hernández-Hernández[1] , E López-Pineda[2] , M E Brandan[2] and Juan Valentín Escobar[1]

[1] Instituto de Física, Departamento de Física Química, Universidad Nacional Autónoma de México 04510, Coyoacán, Mexico City, Mexico
[2] Instituto de Física, Departamento de Física Experimental, Universidad Nacional Autónoma de México 04510, Coyoacán, Mexico City, Mexico

E-mail: escobar@fisica.unam.mx

CrossMark

Abstract

x-rays generated through tribological processes are emitted in fast bursts ($\sim$10 ns) that hinder the correct measurement of the corresponding spectrum. In this work we implement a dosimetry technique based on thermoluminescent materials—impervious to pileup problems arising in solid-state active detectors—to measure the angular distribution of the tribo-generated x-rays from peeling adhesive tape. Unexpectedly, we find evidence of an isotropic energy emission on at least one meridian plane. These results may shed light on the physical processes behind the radiation emission in devices that harness the triboelectric effect to generate x-rays, and prove that dosimetry techniques can be used as an alternative characterization tool in the study of the emission from this and other relatively fast systems.

(Some figures may appear in colour only in the online journal)

1. Introduction

Faraday found back in 1833 that when some dielectric solids are cleaved their surfaces are left electrically charged [1], and even wondered why some electrical discharges generated visible light while others did not [2]. It was later recognized that a fracture process is not necessary for two surfaces originally in intimate contact to become charged upon separation. This phenomenon is nowadays known as contact electrification [3], and it is at the heart of the fact that a dim blue light can be observed with the naked eye when adhesive tape is peeled inside a dark room [4]. It is now recognized that contact electrification is a two-step process: first, during intimate contact, electric charge is transferred until the chemical potential of the bodies are equalized. Second, as the charged surfaces separate abruptly, the electric field between them becomes large enough to cause air breakdown. The freed and subsequently accelerated electrons may then excite and even ionize the

surrounding gas molecules which emit the characteristic nitrogen lines upon relaxation [5]. What Faraday could not have anticipated is that the same basic succession of events involved in the emission of visible light can also yield bremsstrahlung x-rays [6]. This phenomenon is observed, for example, when adhesive bonds–such as those formed by regular adhesive tape–are broken under moderate vacuum ($\sim$10 mTorr). Tribo-generation of x-rays ('TGXs') entails the funneling of mechanical energy into high energy electrons that produce x-rays; in other words, there is no need for an external high-voltage supply [7]. TGXs belong to a broader class of phenomena termed 'Triboluminescence' [8–10], in which a mechanical action such as cleaving [11], peeling [4, 12], rubbing [13], deforming [14] or even sliding [15] produces a flash of light. That triboluminescence can extend over to the x-ray portion of the electromagnetic spectrum was discovered by the Russian school of adhesion in their systematic research about the macroscopic consequences of contact electrification [16]. These

J. Phys. D: Appl. Phys. **53** (2020) 405302

M C Hernández-Hernández *et al*

studies started with Obreimoff's observation in 1930 that cleaving mica sheets in vacuum made the enclosure 'glow like an x-ray tube' [11], continued with the finding that the rupture of adhesive bonds generates high energy electrons by Karasev in 1953 [17] and culminated with Klyuev's measurements of x-ray spectrum from peeling pressure sensitive adhesive tape under vacuum in the 1980s [18, 19]. More recently, it was shown that around 50% of the total x-ray emission happens in bursts lasting only a couple of nanoseconds. Actually, both visible photons [20] and electric currents [21, 22] have also been observed to occur in bursts during the peeling of adhesive tape. The short characteristic time-scales of these bursts is thought to be responsible for the relatively high collimation that allows for x-ray images to be taken with a couple of rolls of commercially available adhesive tape [6, 7]. While the two-step process mentioned above is correct in general, the exact mechanism by which x-rays are emitted is a matter of current debate, including that leading to the fast burst. For example, a portion of the x-ray spectrum measured is consistent with what one would expect from a bremsstrahlung process of electrons with energies between 35 and 50 keV [23, 24], but the angular distribution of the integrated spectrum is not [25]. In this respect, calculating the average energy emitted from the corresponding x-ray spectrum can be problematic, since the nanosecond bursts can lead to pileup events because active solid-state detectors cannot discriminate individual photon energies in such short time-scales [26]. Indeed, our group recently showed that unless the solid angle subtended by CdTe and Si solid-state detectors is at the most 5×10^{-6}, the detected x-ray spectrum will be distorted [23]. Consequently, TGXs spectra from experiments that have overlooked this issue are likely to extend spuriously into higher energies. This may be the case for TGXs generated with either Van der Graaf-type devices [27, 28], tack-type ones (i.e. on and off contact) [29] or tape-peeling itself [6, 24]. Unless properly dealt with, pileup makes the measured spectrum unreliable as a tool for modeling and ultimately understanding the physical processes involved. This extends to the problem of determining the spatial dependency of the average energy of the emission and its comparison with theoretical or simulation results [24, 25]. Such comparison is desirable as it may help gain insight into the physical mechanisms behind TGXs in general and in particular behind the nano-second bursts. To this end, using detection techniques that do not depend on any electronics becomes ideal. One such technique is passive dosimetry [30].

In this work we implement passive dosimetry techniques to determine the angular distribution of x-rays emitted on a meridian plane of TGXs from peeling adhesive tape from its own backing in moderate vacuum. Since the photon intensity measured with this technique is insensitive to pileup or any other effects arising from relatively concurrent x-ray photons, these techniques circumvent the problems associated with conventional solid-state active detectors.

A second advantage of using an array of passive dosimeters for this characterization, is that it eliminates the need to reposition the conventional active solid-state detector on different observation angles, for which breaking the vacuum is usually necessary. To quantify the emitted energy, we use

LiF:Ti,Mg dosimeters (aka TLD100). The TLD100 response as a function of absorbed energy is known to be energy-dependent for energies below 50 keV up to a relative 1.4 factor with respect to the response to cobalt-60 photons [31]. Therefore, in principle, its response should be corrected if the energy distribution were dependent of the observation angle. However, preliminary results recently obtained by our group using CaF$_2$:Tm dosimeters (aka TLD300), suggest that the effective energy of x-rays on the plane studied is independent of the observation angle. In this context, the effective energy of a spectrum (also called equivalent photon energy) is defined as the energy of a monoenergetic beam that has the same half-value layer as the original spectrum [32]. This suggests that the spectrum is indeed independent of the observation angle, and it allows us to interpret the thermoluminescent (TL) signal from the TLD100 dosimeters as being proportional to the photon flux, without corrections related to the energy dependency. We then develop a simple model assuming an isotropic emission of a moving point source and compare its predictions against the experimental flux. Unexpectedly, we find evidence that strongly suggests that the emission is indeed isotropic on at least one meridian plane.

2. Materials and methods

2.1. Tribo-generation of x-rays

TGXs were produced by peeling off-the-shelf pressure-sensitive adhesive tape (Scotch-tape #550, 3M, USA) from its own backing (figure 1). The roll was secured to a ball bearing and peeled by a motor inside a vacuum chamber at 82 rpm. The x-ray spectrum is known to be dependent on gas pressure [23, 24, 33], which rises as the sticky polymer from the tape outgasses when it is being peeled. However, after a transient increase occurring when the motor is switched on, the gas pressure remains steady at 5 mTorr due to the continuous operation of a vacuum pump. The single-photon spectrum from TGXs measured with solid-state detectors under the specified conditions is shown in the inset of figure 1. The detectors were placed right outside of the chamber, at a distance of 8 cm from the ball bearing holding the roll, making an apparent observation angle (as defined in figure 2(b)) close to 0° with respect to the peeling line. To measure this spectrum, the proper measures to suppress pileup were taken (see [23] for details). Knowledge of the spectrum at this observation angle will be used in the discussion section to estimate the attenuation from the adhesive tape itself.

2.2. Dosimetry

Commercially available LiF:Ti,Mg TL dosimeters (Harshaw Chemical Co., USA) with dimensions $3.2 \times 3.2 \times 0.89$ mm^3, commonly referred to as TLD-100 were employed in this study. The dosimeters were sandwiched between two pieces of polyimide tape (24.5 μm thick 'Kapton' tape, DuPont, USA) and secured on an aluminum arch at known distances from the center of the ball bearing. Each dosimeter was labeled according to its observation angle (figure 2(b)). The corresponding
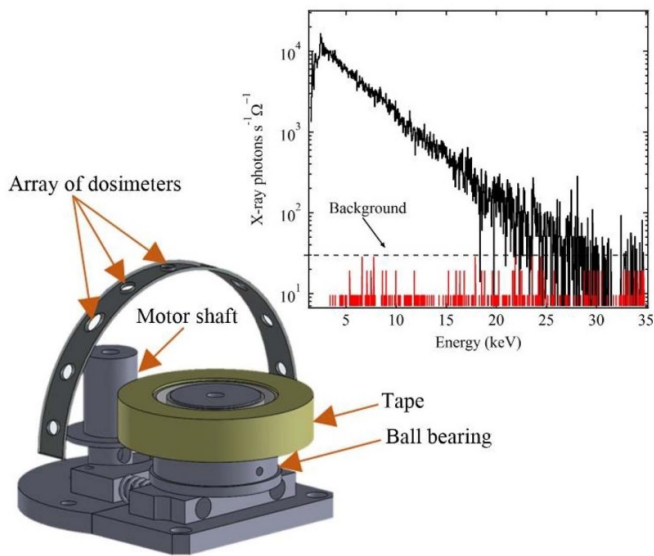
Figure 1. Schematics of the experimental setup. TGXs are produced by peeling off-the-shelf pressure-sensitive adhesive tape from its own-backing inside a vacuum chamber at 5 mTorr of air pressure at 82 rpm. An array of 9 TLD100 dosimeters (sandwiched between two pieces of 25.4 μm thick Kapton tape) are placed at known distances from the source to measure the dose (energy absorbed by each dosimeter per unit mass) on a plane perpendicular to the peeling direction. Inset: single x-ray spectrum measured with a combination of CdTe and Si solid-state detectors at an observation angle of 0° with respect to the center of the ball-bearing onto which the roll of tape is mounted (see figure 2(b)). Black trace in this inset is the average background signal.

meridian plane is perpendicular to the direction of peeling. The energy deposited in the dosimeters was measured following standard procedures in thermoluminescent dosimetry using a dedicated instrument (see next subsection). This instrument generates a TL glow curve for each dosimeter, which represents the amount of emitted light (as measured through the current of a photomultiplier tube) as a function of the dosimeter temperature. The TL reader heats up the dosimeter by a planchet resistive heating, at a constant rate. The integral of the glow curve is proportional to the energy deposited in the dosimeter. This integral is considered as the TL response of the dosimeter. Independent studies [34] have shown that the TL signal of these dosimeters is linear with the deposited energy for doses below 1 Gy.

2.2.1. Dosimeters preparation and readout. 24 h before the irradiations, the dosimeters were annealed at 400 °C for 1 h and then allowed to cool down for 15 min on a metallic surface in thermal equilibrium with a room kept at 18 ± 1 °C. The dosimeters were then annealed at 100 °C for 2 h followed by the same cooling protocol. In TLD-100, the first annealing (at a high temperature) empties the traps and disperses the impurities uniformly in the material, to the original configuration. The second annealing (at a lower temperature) minimizes the contribution of the low-temperature peaks to the glow curve, thus bringing stability against signal fading [35]. After irradiation, the dosimeters were read with a Harshaw 3500

TLD reader in a N_2 enriched atmosphere, at a heating rate of 10 °C s^{-1} from 50 °C to 350 °C. The heating rate is a parameter that affects the shape and the position of the peaks in a glow curve; its precise value is not as important as it is to choose one and always use the same. This, and other parameters of the thermal treatment used in this investigation, are the result of optimization performed earlier in our laboratory to get maximum reproducibility and stability in the readings. To minimize spurious variations due to fading of the low temperature TL signal, readouts were carried out 24 h after irradiation. For each observation angle, the same dosimeter was exposed to TGXs from the peeling of 10 rolls of tape, and then read. This procedure was repeated on 3 different instances for all observation angles, except for the 0° one for which only two exposures were performed. The reliable use of TLD-100 requires that the absorbed dose is greater than a detection threshold, known to be equal to that imparted by about 0.1 mGy air kerma [36]. Finally, concerning the possible dependence of the dosimeter response on the photon angle of incidence [37] we have estimated a maximum angle of incidence of about 10° for the primary x-rays on the chips (zero degrees is the perpendicular incidence on the dosimeter front surface). Two effects might affect the energy deposition by inclined trajectories, namely a longer path inside the dosimeter thickness for inclined trajectories, and a different apparent area presented by the dosimeter, due to its inclination. Analytical calculations of both effects give, for photons up to 10 keV, a dose increased by less than 8% with respect to normal incidence. We did not correct for this effect, considered as minor.

2.3. Isotropic emission model

To construct a model for the x-ray emission, we note that other works have suggested that the flux is proportional to the area of the tape being peeled. Indeed, the emission has been found to be reduced accordingly when mm-wide tape (compared to the commercial cm-wide one) is peeled [38].

In this respect, other studies have also found a dependency of the mean energy on the peeling velocity, a result that was found by analyzing the corresponding integrated x-ray spectra [39]. However, as mentioned in the introduction, the measured spectrum of tribo-generated x-rays is critically dependent on the solid angle subtended by the detector due to possible distortions produced by pileup. Since the work just cited does not specify if the proper measures to suppress pileup were taken, it is possible that the reported spectra are not devoid of distortions. Consequently, this velocity dependence is likely to be spurious as well. Thus, in the model we propose here, we assume the x-ray flux to be velocity-independent and only to be proportional to the area of the tape peeled. Then, if an isotropic emission is assumed, the total energy deposited in each dosimeter (and thus, the TL signal) will be proportional to the solid angle subtended by it with respect to the source, i.e. it will be proportional to the area of the dosimeter A and inversely proportional to the square of its distance to the source, r^2, while also being proportional to the area of tape that has been peeled. As a first-order approximation, we assume the emission is concentrated at a point located midpoint of the contact
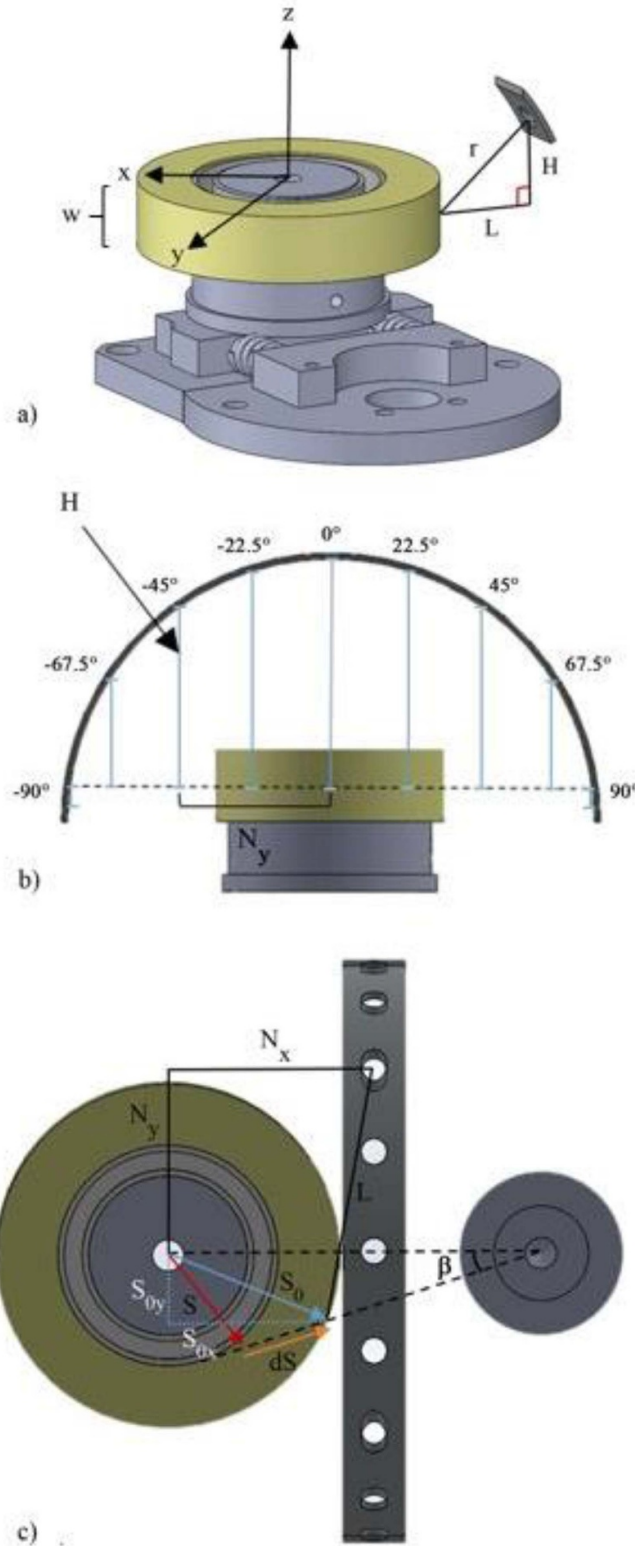
Figure 2. (a) The square of the distance, $|r|^2 = \left|\vec{L}\right|^2 + \left|\vec{H}\right|^2$, from the emission point to a given dosimeter is calculated using the center of the ball bearing as the center of the coordinate system. As a first-order approximation, the emission from the whole contact line is assumed to be concentrated at a point $\vec{S}$ located at the center of the tape's width. (b) Distribution of the dosimeters on the arch: the 'observation angle' is defined as the angle formed between the location of each dosimeter and the center of the roll. (c) As the tape is peeled, $\vec{S}$ moves from its initial position ($\vec{S}_0$, cyan arrow) to a later one (red arrow) on a line defined by the angle $\beta = 18.5°$, allowing for the calculation of the vector $\vec{L}$, provided the coordinates of the dosimeter (N_x, N_y, H) are known. See appendix for details.

line. Now, let α be the total flux per unit area of the tape peeled. Then, we expect the TL signal TLS_n from a dosimeter n placed at a distance r_n to be proportional to the sum of the contributions of the energy emitted during each turn:

$$TLS_n = \sum_{i=0}^{N} \alpha \frac{A}{4\pi r_n^2(i)} P(i) w = \alpha TA_{eff}, \qquad (1)$$

where $P(i)$ is the perimeter of the tape peeled at turn i, $w = 1.2$ cm is its width and $N = 236$ is the total number of turns the roll with undergo (see appendix). Since the perimeter of the roll itself decreases in discrete steps of $2\pi i g$ (where $g = 50$ μm is the tape's backing thickness), r is too a function of i in equation (1). Note that we were able to factor out α in equation (1) precisely because an isotropic emission is being assumed. Furthermore, equation (1) defines an effective area of the tape, TA_{eff}, that can be interpreted as the total area of the tape being peeled from a complete roll reduced by a varying solid angle factor. It is worth pointing out that scattered radiation off the walls may contribute to the dosimeters' signal. Assuming this scattered radiation to be proportional to the primary radiation, this contribution should manifest itself, to a first approximation, as a constant signal for all the dosimeters.

To calculate TA_{eff} in equation (1), the distance of each dosimeter to the emission point must be known as a function of i, in contrast with the case of conventional x-rays sources whose emission point is fixed in space. Given the relatively simple geometry of our setup, it is possible to keep track of this distance analytically. While the details of this calculation are presented in the appendix, here we give an overview. We make use of a coordinate system centered at the axis of the ball bearing (figure 2(a)). Let $\vec{S}_0 = (S_{0x}, S_{0y}, -w/2)$ and $\vec{S}(i)$ be vectors representing, respectively, the position of the original and of the current emission point during the turn i. Given the Z-coordinates of the dosimeters (H, in figure 2(b)), to find r we need only to find the distance L (as defined in figure 2(a)) from the emission point to the X-Y coordinate of the dosimeter placed at $(N_x, N_y, -w/2)$, as shown in figure 2(b). Letting $d\vec{S}(i) = \vec{S}_0 - \vec{S}(i)$ be the difference between these two vectors, it is straightforward to show that the square of the distance from a given dosimeter to the emission point is given by:

$$r^2(i) = H^2 + L^2 = H^2 + \left(S_{0x} - \left|d\vec{S}(i)\right|\cos(\beta) - N_x\right)^2 +$$
$$+ \left(S_{0y} - \left|d\vec{S}(i)\right|\sin(\beta) - N_y\right)^2, \qquad (2)$$

where $\beta = 18.5°$ is the angle formed by the line joining the axes of the ball bearing and the motor shaft, and the location of the contact point (see figure 2(c)). This angle remains constant throughout the entire peeling process. We can then calculate TA_{eff} in equation (1) by plugging the value for $r^2(i)$ from equation (2), given the coordinates of each dosimeter.

To summarize this section, if the emission is indeed isotropic, we expect the dosimeter TL signal to be proportional to TA_{eff}, a simple geometric factor that depends on the location of the corresponding dosimeter.

3. Results and discussion

Figure 3(a) (left axis) shows the results for the TL signal versus observation angle. Each bar is the result of the emission from 10 complete rolls of tape, adding up to about 2500 s of total exposure. In these results we have used the TL response integrated by the TL reader, without need to transform into dose. Independent calibration procedures performed at our laboratory indicate that the doses received by the dosimeters were always larger than those imparted by 5 mGy of air-kerma. These values are well above the detection threshold known for TLD-100 chips. In figure 3(b), we show the averages of these signals. On the right axis of figure 3(b), we plot the values of TA_{eff} from equation (1). The coordinates of the dosimeters that yield these values, along with the corresponding uncertainties can be found on the appendix section. Even at first glance, it is clear in figure 3(b) that TA_{eff}nd the TL signal follow a similar trend, suggesting that the emission is indeed isotropic on this plane. Note, however, that the three data points corresponding to the largest negative angles clearly deviate from the model. As we explain in more detail below, these points correspond to photon paths that are partially blocked by the tape itself.

In figure 3(c) we plot the TL signal versus TA_{eff}. This figure shows that when the points corresponding to large negative angles are not considered, the relation between these variables is well approximated by a linear function, as predicted by the isotropic model of equation (1). The proportionality constant found from the data is $\alpha_{exp} = 0.71 \pm 0.12$, while the ordinate intercept is 0.06 ± 0.26. To better appreciate the systematic deviation of the data to the model for large observation angles, in figure 4(a) we plot the experimental TL signal divided by TA_{eff} for each observation angle and compare against α_{exp} (red horizontal dashed line). Indeed, for the dosimeter located at $-90°$, this ratio is 32% smaller than α_{exp}. While this observation may be interpreted as resulting from the emission being anisotropic, an inspection of the experimental setup (see top view of the setup, figure 4(b)) reveals that, at these angles, the roll of tape partially blocks the photons' path to the dosimeters for a non-negligible portion of the peeling process. Given the typical energies of the x-ray photons involved in this process (inset of figure 1) and the composition of the tape's backing (C_3H_6, polypropylene [40]), a single 50 μm-layer of the tape attenuates the integrated emission already by 10% [41]. Because of the exponential nature of the attenuation process, a 1 mm-path is enough to achieve $\sim$88% attenuation. figure A1 shows that the length of bulk tape x-ray photons must traverse to reach the dosimeter located at $-90°$ is of the order of $dx = 4.65$ mm at the beginning of the peeling process. For smaller negative angles, this path will be progressively smaller until it is minimized for some observation angle close to $0°$. In contrast, to reach the dosimeter at $+90°$ photons need only to go through a single layer of tape. This asymmetry is precisely what we observe qualitatively in figure 4(a). We can go one step further and assess if this explanation makes sense quantitatively too, as follows. Let N_{block} be the number of turns during which there existed any obstruction of the x-rays path to these dosimeters, and N_{free} the remaining turns. Making the simplifying assumption that during the first N_{block} turns there
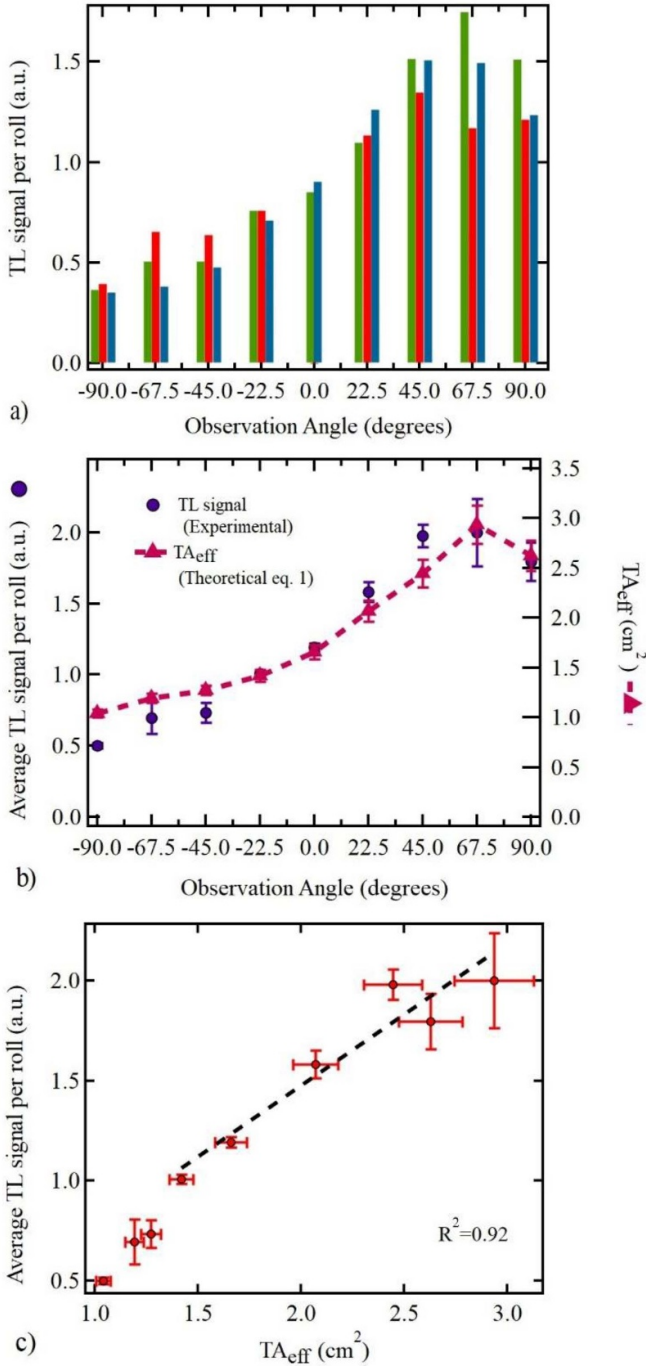
a)

b)

c)

Figure 3. (a) Dosimeter TL signal. (b) Average TL signal (dots, left axis) measured experimentally and tape's effective area (triangles, right axis) obtained theoretically (equation (1)). Error bars in the TL signal are the standard deviations of the values shown in (a), which is larger than the estimated uncertainty of 5% of each individual experiment. (c) Linear fit between the experimental average TL signal per roll and the effective area obtained with equation (1).

is 100% attenuation and 0% for the rest, an upper limit to the expected attenuation is given by

$$\frac{1 * TA_{eff}(0, N_{block}) + 0 * TA_{eff}(N_{block}, N_{free})}{1 * TA_{eff}(0, N)} = \frac{TA_{eff}(0, N_{block})}{TA_{eff}(0, N)}$$
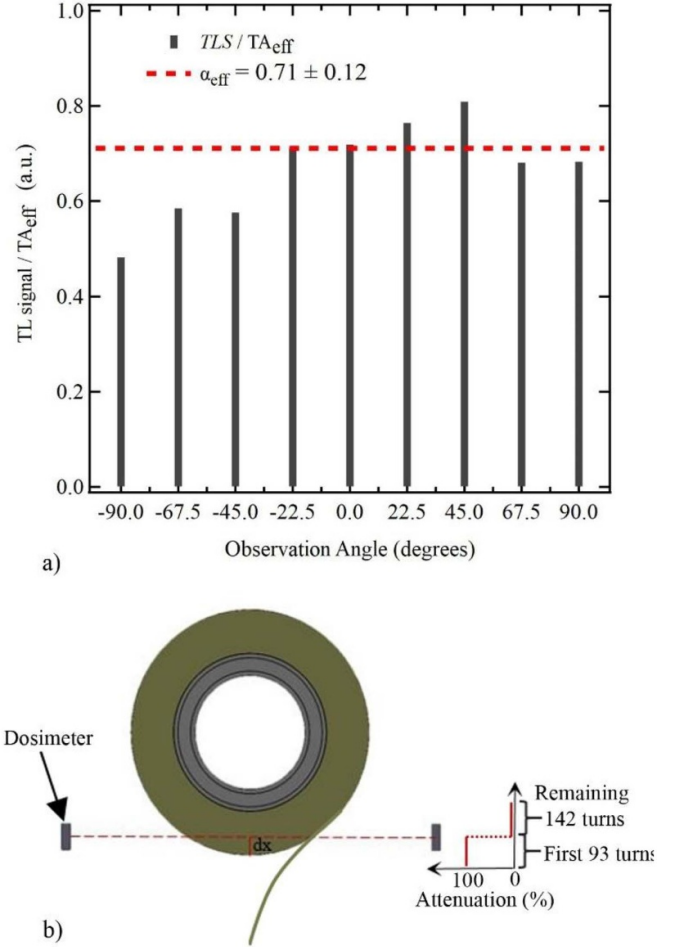
(3)

a)

b)

Figure 4. (a) Dosimeters' TL signal divided by TA_{eff} as a function of the observation angle compared to the proportionality factor from the isotropic model (α_{exp}, red dotted line) that best fits the data. (b) Schematic top view of the roll of tape showing how the tape partially blocks the photons' paths towards the dosimeters located at large observation angles. The attenuation plot (lower right corner) serves as a simplified model suggesting that tape attenuation is the source of the deviations of the experimental data from α_{exp} in (a).

where the effective area (as defined in equation (1)) has been written as an explicit function of the initial and final number of turns, $TA_{eff}(i_i, i_f)$. Given that a portion $dx = 4.65$ mm of the radius of the roll of tape that blocks this path (approx. 16% of the total radius, figure 4(b)), and using a similar expression as the one used to find the total turns N (see appendix), we find $N_{block} = 93$ and $N_{free} = N - N_{block} = 143$. Plugging these values into equations (1) and (3), yields an attenuation of 43%, which is reasonably close to the 1/3 attenuation observed, especially considering the crudeness of the model. Thus, the observed deviations of the ratio (TLS/TA_{eff}) from a constant as reported on figure 4(a) are likely the result of this partial obstruction.

Based on this analysis and on the results of figures 3(a) and (b), we conclude that emission from this radiation source is isotropic, at least on the plane studied.

One possible explanation for the isotropic emission found is a lack of preferential direction on the electron emission that generates bremsstrahlung radiation. In this respect, an inspection of the peeling vertex with a microscope [42] shows

that a rather messy mesh of sticky stings forms during the peeling process that may be mediating the discharge process. This mesh may be randomizing the path of the electrons released to a large extent. A similar explanation could support the assumed angular independence of the effective x-ray energy mentioned in the introduction. It would be interesting to investigate if the emission is isotropic too in other tribo-generators that use dry friction as opposed to peeling sticky tape. Finally, we note that the contribution from scattered radiation (given by the y-intercept of the linear fit in figure 3(c), 0.06) to the total signal (on the order of 1) is small. However, the uncertainty associated to the ordinate intercept is many times larger than its average value. More statistics would be necessary to establish if this contribution is indeed small. In this same respect and given the challenges that tape attenuation imposes, it may be more appropriate to implement a new arrangement that measures scattered radiation exclusively to correctly assess the contribution of secondary radiation on the results presented. This could be achieved, for example, by placing dosimeters on the outer face of the metallic arch so that the view from the primary source is blocked. This study will be carried out in a follow-up investigation.

4. Concluding remarks

We have found evidence that supports the theory of an isotropic emission from TGXs from peeling adhesive tape on at least one meridian plane. Considering that this plane was chosen arbitrarily, it is possible that this isotropy extends to the rest of the meridians.

The success of using dosimetry techniques applied to this system would make it straightforward to investigate if the emission is indeed isotropic over a whole hemisphere with a resolution limited by the size of dosimeters. This investigation is underway, as well as the evaluation of the effective energy at different emission angles.

We end by emphasizing that the model we have presented in this work rests on the assumption of similar effective energy for the x-ray emitted on the studied plane. If this were not the case, the TLD100 signal could not be assumed to be proportional to the absorbed dose.

Acknowledgments

Appendix

In equation (1), knowledge of the length of segment $|d\vec{S}|$ is necessary to calculate r^2. We now refer to figure A1 for this derivation. As mentioned in section 2.3, the angle β is
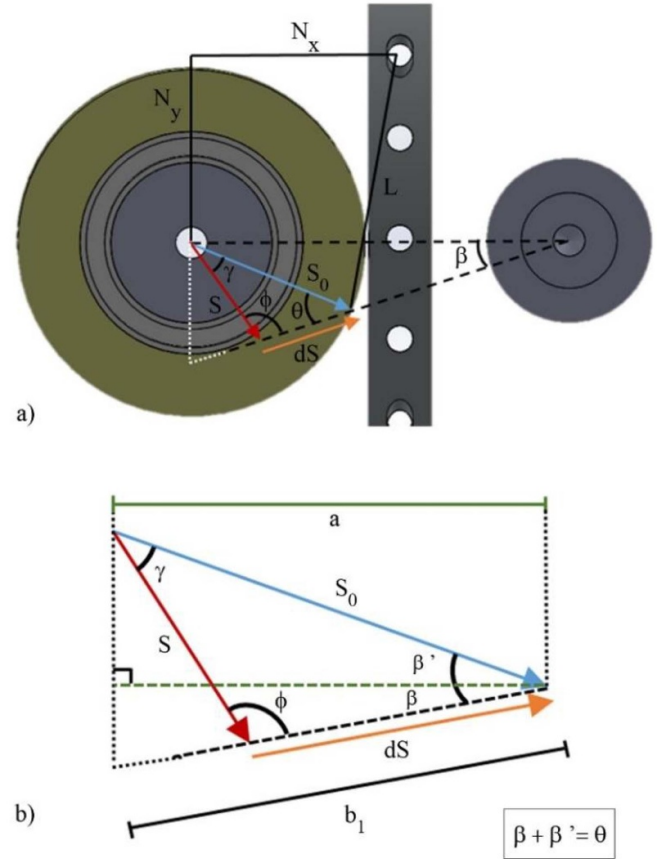

Figure A1. (a) Schematic diagram of the position of the contact line. The angles γ, θ and ϕ, are formed by the vectors $\vec{S}$ (red arrow), $\vec{S}_0$ (cyan arrow) and $d\vec{S}$ (orange arrow). (b) Close-up of (a), defining the angles β and β', as well as the distances a (green solid line) and b_1 (black solid line) used to calculate $|d\vec{S}|$ (equation (A3)), and from it, calculate r^2 (equation (2)). In these figures, the dashed line parallel to $d\vec{S}$ becomes a dotted one at the point where the tape ends.

constant throughout the peeling process and is defined (see figure A1(a)) as that formed between the line connecting the center of the ball bearing and the center of the motor shaft, and the vector $|d\vec{S}|$. We calculate $|d\vec{S}|$ using the law of sines for the angles shown in figure A1(a):

$$\frac{\left|\vec{S}\right|}{\sin(\theta)} = \frac{\left|\vec{S}_0\right|}{\sin(\phi)} = \frac{\left|d\vec{S}\right|}{\sin(\gamma)}. \tag{A1}$$

This relation can be better appreciated by looking at a close-up of the triangle formed by the three vectors $d\vec{S}$, $\vec{S}$ and $\vec{S}_0$ (figure A1(b)).

We first calculate the angles β and β' that sum up to θ. These angles are obtained through the relations: $\cos(\beta) = a/b_1$ and $\cos(\beta') = a/|\vec{S}_0|$, where the distances a, b_1 and $|\vec{S}_0|$ are measured a priori. From these equations, we find $\theta = 33.52°$. Solving for ϕ in equation (A1), we obtain:

J. Phys. D: Appl. Phys. **53** (2020) 405302

M C Hernández-Hernández *et al*

Table A1. Effective area and corresponding uncertainties for each dosimeter using equations (1), (2), A1, A2 and A3. For these calculations, the following measured constants were used: $\beta = 18.5°$, $N_x = 2.3$ cm, $S_{0x} = 2.77$ cm, $S_{0y} = -0.55$ cm, $w = 1.25$ cm, $g = 50$ μm, $A = 0.09$ cm^2 and $N = 236$. An uncertainty of 1 mm was assigned to the measurement of r (δr), from which the uncertainty in r^2 was calculated through the relation $\delta r^2 = 2r\delta r$. In turn, this yields an uncertainty of $\delta TA_{eff} = TA_{eff}\delta r^2/r^2$ in the effective area. The values of TA_{eff} along with the corresponding uncertainties (5th and 6th columns) are the ones displayed in figure 3.

Dosimeter #n	Angle	H (cm)	N_y (cm)	TA_{eff} (cm^2)	TA_{eff} Uncertainty (cm^2)	Average TL signal per roll (a.u.)	TL signal standard deviation (a.u.)
1	$-90°$	0.086	4.43	1.043	0.037	0.50	0.024
2	$-67.5°$	1.51	3.85	1.19	0.044	0.70	0.15
3	$-45°$	2.86	2.96	1.27	0.049	0.73	0.096
4	$-22.5°$	3.61	1.83	1.42	0.059	1.008	0.032
5	0	3.99	0.20	1.66	0.076	1.19	0.035
6	22.5°	3.61	-1.43	2.07	0.11	1.58	0.096
7	45°	2.86	-2.56	2.44	0.14	1.98	0.11
8	67.5°	1.51	-3.45	2.93	0.19	2.00	0.32
9	90°	0.086	-4.03	2.63	0.15	1.79	0.19

$$\phi = \pi - \arcsin\left(\left|\vec{S}_0\right|\sin(\theta)/\left|\vec{S}\right|\right) \quad (A2)$$

where we have added π to the RHS since ϕ is an obtuse angle. Recalling that the radius of the roll changes as a function of the number of turns i, we substitute $|\vec{S}|$ in equation (A2) for $|\vec{S}| = (|\vec{S}_0| - i\,t)$, where, as before, t is the thickness of the tape. This allows us to calculate the remaining angle, $\gamma = \pi - \theta - \phi$, and finally solve for $|d\vec{S}|$ in equation (A1):

$$\left|d\vec{S}\right| = \frac{\left|\vec{S}_0\right|\sin(\gamma)}{\sin(\phi)} \quad (A3)$$

which, indirectly, is a function of i. In table (A1), we display the values for TA_{eff} for each dosimeter given their coordinates using equations (1), (2), (A2) and (A3). Finally, to calculate the total number of turns N the roll will undergo given its total length, we perform the following calculation. The total length of a roll of tape of the particular brand used in these experiments is 3300 cm, so that the total number of turns N that the roll will undergo is obtained by solving for this variable when adding up the individual perimeters of each turn: $\sum_{i=0}^{N} P(i) = \sum_{i=0}^{N} 2\pi(|\vec{S}_0| - ig) = 2\pi|\vec{S}_0|(N+1) - \pi g N(N+1) = 3300$. From this relation, we obtain $N = 236$ turns.

ORCID iDs

M C Hernández-Hernández ⬚ https://orcid.org/0000-0002-1755-1955
E López-Pineda ⬚ https://orcid.org/0000-0002-1304-0058
M E Brandan ⬚ https://orcid.org/0000-0002-1165-3440
Juan Valentín Escobar ⬚ https://orcid.org/0000-0001-6048-2011

References

[1] Faraday M 1833 *Phil. Trans. Royal Soc. London* **123** 23–54
[2] Faraday M 1838 *Phil. Trans. Royal Soc. London* **128** 125–68
[3] Harper W R 1967 *Contact and Frictional Electrification* (Oxford: Oxford University Press)
[4] Harvey E 1939 *Science* **89**
[5] Raizer Y 1991 *Gas Discharge Physics* (New York: Springer)
[6] Camara C G, Escobar J V and Hird J 2008 *Nature* **455** 1089
[7] Putterman S, Camara C G, Escobar J V and Hird J 2014 *US Patent* 8699666
[8] Walton A J 6 1977 *Adv. Phys.* **26** 887–948
[9] Xie Y J and Li Z 5 2018 *Chem* **4** 943–71
[10] Olawale D O, Dickens T, Sullivan W G, Okoli O I, Sobanjo J O and Wang B 2011 *J. Lumin.* **131** 1407–18
[11] Obreimoff J W 1930 *Proc. R. Soc.* A **127** 290
[12] Donaldson E E, Dickinson J T and Shen X A 1986 *J. Adhes.* **19** 267–86
[13] Bacon F 1640 *Of the Advancement and Proficience of Learning* (Menifee, CA: Flamingo)
[14] Moon Jeong S, Song S, Lee S K and Choi B 5 2013 *Appl. Phys. Lett.* **102** 051110
[15] Picard J 1676 *Mem. Acad. Roy. Sci.* **2** 202–3
[16] Deryaguin B V, Krotova N A and Smilga V P 1978 *Adhesion of Solids* (New York: Consultants Bureau)
[17] Karasev V V, Krotova N A and Deryagin B W 1953 *Akad. Nauk. SSR* **88** 777–80
[18] Klyuev V A 1984 *Soviet Tech. Phys. Lett.* **10** 480
[19] Klyuev V A, Toporov Y, Aliev A D, Chalykh A E and Lipson A G 1989 *Soviet Phys. Tech. Phys.* **34** 361
[20] Ma Z Y, Fan J W and Dickinson J T 1988 *J. Adhes.* **25** 63–77
[21] Lee S, Jensen L C, Langford S C and Dickinson J T 1 1995 *J. Adhes. Sci. Technol.* **9** 1–26
[22] Scudiero L, Dickinson J T, Jensen L C and Langford S C 1 1995 *J. Adhes. Sci. Technol.* **9** 27–45
[23] Hernández-Hernández M C and Escobar J V 2019 *Appl. Phys. Lett.* **115** 201605
[24] Krämer D, Lutzenkirchen-Hecht D, Luhmann B, Keite-Telgenbuscher K and Frahm R 2013 *Rev. Sci. Inst.* **84** 7
[25] Constable E, Horvat J and Lewis R A 2010 *Appl. Phys. Lett.* **97** 131502
[26] Taguchi K, Frey E C, Wang X L, Iwanczyk J S and Barber W C 2010 *Med. Phys.* **37** 3957
[27] Van Cleve E *et al* 2015 *Proc. SPIE* **9590** 95900F
[28] Camara C G, Hird J R and Putterman S J 2015 *US Patent* 9089038
[29] Hird J R, Camara C G and Putterman S J 2011 *Appl. Phys. Lett.* **98** 133501
[30] Bartlett D T 2008 *Radiat. Meas.* **43** 133–8
[31] Scarboro S B, Followill D S, Howell R M and Kry S F 2011 *Med. Phys.* **38** 2619–28

J. Phys. D: Appl. Phys. **53** (2020) 405302

M C Hernández-Hernández *et al*

[32] Attix F H 1986 *Introduction to Radiological Physics and Radiation Dosimetry* (University of Winsconsin Medical School Madison)

[33] Escobar J 2009 *Doctoral Dissertation* University of California

[34] Moscovitch M and Horowitz Y S 2006 *Radiat. Meas.* **41** S71–7

[35] Horowitz Y S 1990 *Radiat. Prot. Dosimetry* **30** 219–30

[36] de Vries W and Bos A J J 1990 *Radiat. Prot. Dosimetry* **33** 251–3

[37] Al-Senan R M and Hatab M R 2011 *Med. Phys.* **38** 4396–405

[38] Camara C G, Escobar J V, Hird J R and Putterman S J 2010 *Appl. Phys.* B **99** 613

[39] Stöcker H, Rühl M, Heinrich A, Mehner E and Meyer D C 2013 *J. Electrostat.* **71** 905–9

[40] Krämer D 2018 *Doctoral Dissertation* Universität Wuppertal, Faculty of Mathematics and Natural Sciences

[41] NIST National Institute of Standards and Technology (https://physics.nist.gov) (Accessed: 20 September 2019)

[42] Nature Videos 2008 (https://www.youtube.com/watch?v=LQBjRF9mX1Y&t=350s) (Accessed: 9 December 2019)